Acta metall. mater. Vol. 38, No. 11, pp. 2073–2083, 1990
Printed in Great Britain. All rights reserved

0956-7151/90 \$3.00 + 0.00

SURFACE FORCES AT CRACK INTERFACES IN MICA IN THE PRESENCE OF CAPILLARY CONDENSATION

KAI-TAK WAN† and B. R. LAWN

Ceramics Division, National Institute of Standards and Technology, Gaithersburg, MD 20899, U.S.A.

(*Received* 28 *December* 1989; *in revised form* 4 *May* 1990)

Abstract—A fracture mechanics model for brittle cracks with capillary condensation is developed. The model is based on an integration of intersurface forces, comprising solid–liquid–solid forces within the capillary and solid–vapour–solid forces without. The work of adhesion thus contains terms from these two regions of the adhesion zone, plus a term from the surface tension of the meniscus. Three interface types are considered: virgin, corresponding to first propagation of the crack through the bulk solid; healed–matched, corresponding to *re*propagation after crack retraction of a partial cleavage; and healed–misoriented, where the cleavage halves are first fully separated and rotated before closure. Notwithstanding the possibility that a layer of environmental molecules may become trapped on interfacial closure, thereby reducing the intrinsic cohesion, we predict the work of separation for healed-matched interfaces to have the same dependence on partial pressure of interactive environmental species as for virgin interfaces, provided lattice coherence is maintained between the matching surfaces. A different dependence is predicted for healed-misoriented surfaces, because of the loss of such coherence, in which case the greater part of the adhesion comes from the liquid surface tension. Results of equilibrium cleavage experiments on mica in water vapour confirm these predictions. The strongly increasing work of adhesion observed for virgin and healed-matched surfaces with diminishing relative humidity is indicative of a long-range, Coulombic component of bonding in the pristine mica structure. Implications of the results in the general description of brittle fracture, and of contact adhesion, are discussed.

Résumé—Nous avons développé un modèle de mécanique de la rupture pour les fissures fragiles dans le cas de la condensation capillaire. Ce modèle est basé sur une intégration des forces entre les surfaces, comprenant les forces solide–liquide–solide à l'intérieur du capillaire et les forces solide–vapeur–solide à l'extérieur. Le travail d'adhésion contient donc des termes provenant de ces deux régions de la zone d'adhésion, plus un terme provenant de la tension superficielle du ménisque. On considdère trois types d'interfaces: interface vierge, correspondant à la première propagation de la fissure à travers le solide massif; interface cicatrisée, correspondant à une seconde propagation après le retrait de la fissure d'un clivage partiel; interface cicatrisée avec désorientation, quand les deux parties clivées ont été complètement séparées et tournées l'une par rapport à l'autre avant fermeture. Bien qu'il soit possible qu'une couche de molécules de l'environnment soit piégée sur las fermeture interfaciale—ce qui réduit la cohésion intrinsèque—nous prédisons que le travail de séparation pour les interfaces cicatrisées dans désorientation dépend de la pression partielle des espèces interactives de l'environnement de la meme manière que le travail de sortie pour les interfaces vierges, à condition que la cohérence du réseau soit maintenue entre les surfaces accolées. Une loi différente est prédite pour les surfaces cicatrisées avec désorientation parce que cette cohérence est perdue; dans ce cas, la majeure partie de l'adhésion provient de la tension superficielle du liquide. Les résultats des expériences de clivage à l'équilibre réalisées sur le mica exposé à de la vapeur d'eau confirment ces prévisions. Le fort accroissement du travail d'adhésion, observé pour les surfaces vierges et cicatrisées lorsque l'humidité relative diminue, témoigne d'une composante à longue distance de type coulombien pour la liaison dans la structure parfaite du mica. Nous discutons les implications de ces résultats sur la description générale de la rupture fragile et de l'adhésion de contact.

Zusammenfassung—Ein bruchmechanisches Modell wird für Sprödrisse mit kapillarer Kondensation entwickelt. Das Modell fußt auf einer Integration von Kräften zwischen Oberflächen, fest-flüssig-feste Kräfte innerhalb der Kapillare und fest-dampfförmig-feste-Kräfte ohne Kapillare. Die Adhäsionsarbeit enthält daher Terme dieser beiden Bereiche der Adhäsionszone plus einem Term durch die Oberflächenspannung des Meniskus. Drei Grenzflächentypen werden betrachtet: der jungfräuliche, entsprechende der ersten Bewegung des Risses durch das Festkörpervolumen; der passend-ausgeheilte, entsprechend der *Wieder*-ausbreitung nach teilweisem Rißrückschritt; der ausgeheilt-fehlorientierte, bei dem die Rißflächen erst getrennt sind und fehlorientiert wieder zusammengefügt werden. Trotz der Möglichkeit, daß eine Schicht von Molekülen aus der Umgebung bei der Rißschließung eingefangen werden können, wobei die intrinsische Kohäsion verringert wird, sagen wir voraus, daß die Trennungsarbeit der passend-ausgeheilten Grenzflächen dieselbe Abhängigkeit vom Partialdruck der wechselwirkenden Spezies aus der Umgebung aufweisen wie bei der jungfräulichen Grenzfläche, vorausgesetzt, zwischen den passenden Oberflächen bleibt die Gitterkohärenz erhalten. Eine andere Abhängigkeit wird für die ausgeheilt-fehlorientierten Oberflächen wegen des Verlustes einer solchen Kohärenz, bei dem der größere Teil der Adhäsion von der Oberflächenspannung der Flüssigkeit kommt, vorausgesagt. Ergebnisse von Versuchen zur Spaltung von Glimmer im Gleichgewicht in Wasserdampf bestätigen diese Voraussagen. Die stark zunehmende Adhäsionsarbeit, die bei jungfräulichen und passend-ausgeheilten Oberflächen mit verschwindender Feuchtigkeit beobachtet wurde, weist auf weitreichende Coulombkomponenten der Bindung in der ursprünglichen Glimmerstruktur hin. Die Bedeutung der Ergebnisse für die allgemeine Beschreibung des Sprödbruches und der berührungsadhäsion werden diskutiert.

†Doctoral Student, Department of Materials Science and Engineering, Lehigh University, Bethlehem, PA 18015, U.S.A.

1. INTRODUCTION

The deleterious effects of interactive environments, especially moisture, on the resistance to crack propagation in mica [1–10] and other intrinsically brittle materials like silicate glasses [11, 12] and sapphire [12, 13] have been well documented. Intrusion of environmental species into the crack effectively reduces the energy of separation W, by lowering the intersurface cohesion. Brittle fracture is in fact one of the few practical routes to evaluation of W. In a fracture experiment, a variation in this quantity is manifested as a corresponding variation in the crack length at which the system under sustained loading maintains a state of equilibrium [14].

Recently, a theoretical description of crack interfaces which expresses the work of separation in terms of "surface forces" has been proposed [10, 15–18]. The description is based on the fundamental notion that W is determined uniquely by the area under the constitutive interplanar stress–separation curve. Contributions to the surface force function from competing sources then appear as superposable quantities in a unifying formalism, in the manner of Derjaguin's concept of "disjoining pressure" [19]. Especially appealing is the prospect that such a surface force function might be amenable to direct measurement, e.g. as is done for mica in the now-celebrated crossed-cylinder apparatus of Israelachvili [20]. The description also has inbuilt provision, through the existence of metastable interface states, for explaining the reduced work of separation at healed, as opposed to virgin interfaces, in terms of occlusion of environmental species at the closed crack [10, 16, 17].

One element that appears not to have received detailed theoretical attention in the context of brittle fracture is that of capillary condensation at the crack interface. This is somewhat surprising in view of the fact that most pristine surfaces are readily wetted by water. Indeed, direct observations of capillary condensation at crack interfaces have been reported in the fracture literature, e.g. in mica [6]. We cite a simple crack simulation experiment in which two otherwise non-adhering glass strips with intervening thin film of wetting liquid are peeled apart [21]: there, measurement of the mechanical energy expended in propagating the crack is readily demonstrated to equal (twice) the surface energy of the liquid, consistent with adhesion exclusively from the Laplace pressure [22]. The allusion is that capillary forces can be a significant factor in the adhesion of interfaces in brittle solids, especially in moist environments, and even dominant where the intrinsic solid–solid bonding is weak.

Accordingly, in this paper we expand the previous surface force model [10] to incorporate capillary condensation. Our analysis is analogous to that described by Derjaguin *et al.* [23] for two non-contacting solid spheres with a liquid "bridge". We consider crack propagation through three interface types: *virgin*—cleavage surfaces bonded by bulk solid–solid cohesive forces; *healed–matched*—surfaces opened in presence of adsorptive environmental species and recontacted in lattice registry; *healed–misoriented*—surfaces again opened in presence of environment but recontacted after mutual rotation about a common surface normal. The results of clevage experiments on mica in moist environments over a range of relative humidities are used to confirm the essential predictions of the model. We conclude that prevailing theories of environmentally-enhanced brittle-crack propagation, based for instance on reduction of intersurface forces by adsorption [13, 24], dielectric screening [25], or negation of surface charge [2, 23], are inadequate, and that the capillary term is in fact indispensable in explaining the adhesion.

An interesting facet of the present work is its relevance to contact adhesion. Contact experiments between curved surfaces constitute an alternative, much travelled route to the measurement of adhesion energies, notably in elastomer–glass systems [26, 27] and mica–mica in the Israelachvili apparatus [28]. Environmentally-induced variations in W are reflected as changes in the pulloff force [29, 30]. Theoretically, there is an inherent "equivalence" between adhesive contact and brittle fracture, insofar as the surface force functions which determine the interface geometry in the respective contact-circle and crack-front regions may be assumed to be the same [10, 17, 18, 27, 31]. However, the contact experiment is restrictive in that it involves two independently prepared surfaces: accordingly, it provides information only on healed–misoriented surfaces, or at best (with special care in specimen alignment) on healed–matched surfaces [32]; it is not suited to determining the primary bonding component of the surface force function that characterises the virgin interface. There are further restrictions associated with the typically small scale of the contact area in relation to the adhesion zone, which we shall describe in Section 4. On the other hand, the importance of capillary condensation has been explicitly demonstrated in contact adhesion experiments [33, 34], although only for configurations where the capillary is the principal source of interfacial interaction.

As a result of these considerations, we shall be led to suggest that the fracture experiment gives a more comprehensive picture of the total adhesion, including a contribution to the attractive surface force function from the Coulombic bonding responsible for the intrinsic strength of the virgin mica crystal. At healed interfaces, we shall also see that lattice coherence is at least as important a factor in determining interface energy in mica as is exposure to interactive chemical species during the closure.

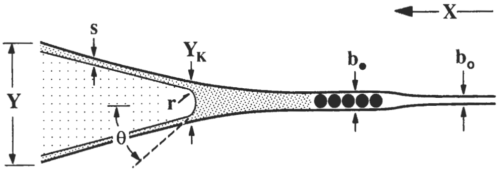

Fig. 1. Crack interface with adsorption layer s, capillary of Kelvin radius r and contact angle θ. Coordinates X, Y locate atom planes bounding the cleavage plane, with equilibrium spacing b_O at virgin interface and $b_\bullet$ at healed-occluded interface, and opening Y_K at meniscus.

2. THEORY

We first develop a theoretical surface force description for the adhesive interaction of two surfaces across a crack (or contact) interface in thermal and chemical equilibrium with a condensable vapour, such that a capillary forms at the narrow interface. To avoid potential complications associated with large-scale capillary zones (recall our allusion in Section 1 to the restriction associated with small contact areas), we focus on the limiting condition of "long" cracks, i.e. crack length≫capillary length. This limiting condition is almost invariably satisfied in brittle fracture experiments, certainly in the experiments to be described in the next section.

In this limit we may make use of a powerful fracture mechanics theorem, due to Rice [35], called the J-integral. This theorem is especially well suited to evaluating the mechanics of straight-fronted cracks with distributed intersurface stresses $\sigma(X)$, with X a crack-plane coordinate measured from an origin where $\sigma(0) = 0$, Fig. 1. The theorem defines a quantity J which can be expressed as a contour integral over the lower and upper crack surfaces

$$J = \int_0^\infty \sigma(X)(\partial Y/\partial X)\,\mathrm{d}X = \int_b^\infty \sigma(Y)\,\mathrm{d}Y \tag{1}$$

at equilibrium, where $\sigma(Y)$ is the attractive surface force per unit area of crack plane at separation Y and b is the intersurface separation at $X = 0$. For small adhesion zones in linear elastic bodies, J identifies with the so-called Griffith–Irwin mechanical-energy-release rate G [14]

$$J = G(c) = -\mathrm{d}U_\mathrm{M}/\mathrm{d}c \tag{2}$$

with U_M the mechanical energy (stored elastic energy plus potential energy of applied load) per unit width of crack front and c the crack length. The area under the σ–Y curve defines the Dupré work of adhesion in environment E

$$W_\mathrm{E} = \int_b^\infty \sigma(Y)\,\mathrm{d}Y \tag{3}$$

which is identical with the right-hand side of equation (1). Hence the result is self-consistent with the familiar Griffith condition for equilibrium cracks [14], i.e. $G_\mathrm{c} = W_\mathrm{E}$.

A feature of the J-integral is that solutions may be obtained without having to specify the form of the surface force function $\sigma(X)$, or of the corresponding crack-interface geometry $Y(X)$. The adhesion energy in equation (3) simply represents the difference between initial and final states along a reversible path in σ–Y space [10]. The *initial*, bonded state ("closed" interface) at $Y = b$ depends on the formation history: e.g. whether the interface is in its virgin or healed state; and, in the latter case, on the presence of any occluded environmental species and on any lattice incoherence between recontacted surfaces. The *final*, free-surface state ("open" interface) at $Y = \infty$ depends only on the immediate environment.

2.1. General formulation for interface with capillary condensation

Let us now apply the J-integral formalism to an equilibrium crack with capillary condensation, as shown in Fig. 1. We suppose that the capillary extends back to the point where the crack-opening displacement Y_K is equal to

$$Y_\mathrm{K} = 2(s + r\cos\theta) \quad (Y_\mathrm{K} > b) \tag{4}$$

s is the thickness of adsorbed layer on each crack wall, governed by some adsorption isotherm $s = s(p)$ [36], where p is the vapour pressure (or partial pressure of active species in a mixed atmosphere); θ is the contact angle; r is the Kelvin radius [36]

$$r = \gamma_\mathrm{LV} v_\mathrm{M}/kT \ln(p_\mathrm{s}/p) \tag{5}$$

with γ_LV the surface energy of the liquid in equilibrium with its vapor, v_M the molecular volume, k Boltzmann's constant, T absolute temperature, and p_s the pressure at saturation. A plot of $r = r(p)$ vs $RH = p/p_\mathrm{s}$ for water using $\gamma_\mathrm{LV} = 72\ \mathrm{mJ\cdot m^{-2}}$ [36] is shown in Fig. 2. It is apparent from these considerations that $Y_\mathrm{K} = Y_\mathrm{K}(p)$, i.e. the size of the capillary zone depends on pressure p. For a wetting condensate ($\theta < 90°$), the capillary extends down the ever-confining interface until the constraint of the walls precludes further penetration of the

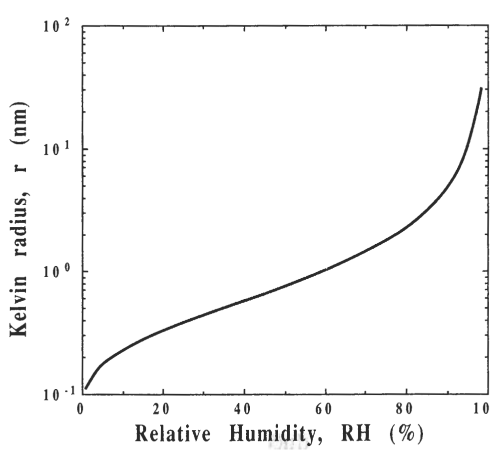

Fig. 2. Plot of Kelvin radius r as function of relative humidity $\mathrm{RH} = p/p_\mathrm{s}$ of water vapour at $T = 300$ K.

Table 1. Notation used for important quantities in text

Variables		
Energy	W	work of adhesion
	U	potential energy
	γ	interface (surface) energy
Force/area	σ	surface force
	p	partial pressure
Dimension	Y	intersurface separation
	b	lattice spacing
Subscripts/superscripts		
Medium	0	vacuum
	L	liquid
	V	vapour
Interface type	v	virgin
	h	healed–matched
	ϕ	healed–misoriented
Energy state	i	initial
	f	final
	K	Kelvin
Closed interface	○	non-occluded
	●	occluded

constituent molecules at $Y = b_\bullet$ [17, 18]. Within the (cylindrical) capillary a negative Laplace hydrostatic pressure [36]

$$\sigma_{\mathrm{Lap}} = \gamma_{\mathrm{LV}}/r \quad (2s < Y < Y_{\mathrm{K}}) \tag{6}$$

acts to close the crack walls. Ahead of the point of maximum penetration the walls narrow down asymptotically to $Y = b_\circ$, just as if they were in vacuum.

Now let us evaluate the work of adhesion for the crack in Fig. 1 at constant humidity ($dp = 0$), without regard at this stage as to whether we are dealing with virgin or healed interfaces, by expanding equation (3) as follows

$$W_{\mathrm{V}} = \int_b^{Y_{\mathrm{K}}} (\sigma_{\mathrm{L}} + \sigma_{\mathrm{Lap}})\,\mathrm{d}Y + \int_{Y_{\mathrm{K}}}^{\infty} \sigma_{\mathrm{V}}\,\mathrm{d}Y \tag{7}$$

where L and V in the intersurface stress function $\sigma(Y)$ refer to liquid and vapour environments. Noting the pressure dependence of Y_{K} and σ_{V}, and integrating the σ_{Lap} term in equation (7) using equations (4) and (6), we have

$$W_{\mathrm{V}}(p) = \int_b^{Y_{\mathrm{K}}(p)} \sigma_{\mathrm{L}}\,\mathrm{d}Y + \int_{Y_{\mathrm{K}}(p)}^{\infty} \sigma_{\mathrm{V}}(p)\,\mathrm{d}Y + 2\gamma_{\mathrm{LV}}\cos\theta. \tag{8}$$

It is convenient to define the analogous energies of adhesion in vacuum (0) and liquid

$$W_0 = \int_b^{\infty} \sigma_0\,\mathrm{d}Y \tag{9a}$$

$$W_{\mathrm{L}} = \int_b^{\infty} \sigma_{\mathrm{L}}\,\mathrm{d}Y. \tag{9b}$$

Then equation (8) reduces to

$$W_{\mathrm{V}}(p) = W_{\mathrm{L}} + 2\gamma_{\mathrm{LV}}\cos\theta + I(p) \tag{10}$$

where the last term is a residual integral of surface force functions outside the meniscus

$$I(p) = \int_{Y_{\mathrm{K}}(p)}^{\infty} [\sigma_{\mathrm{V}}(p) - \sigma_{\mathrm{L}}]\,\mathrm{d}Y. \tag{11}$$

Equation (10) indicates that the equilibrium work of adhesion in vapour is greater than that in a wetting liquid by an amount determined by the surface tension of the liquid at the meniscus and (long-range) surface forces beyond.

Thus far our formulation for W is quite general: we have not given explicit attention to virgin, healed-matched and healed-misoriented interfaces; nor have we identified the appropriate initial and final energy states that control this quantity. In making such distinctions, we adopt the notations summarised in Table 1: v (virgin), h (healed-matched), and ϕ (healed-misoriented) denote specific interface type; i, f and K initial, final and Kelvin (intermediate) energy states; ○ and ● closed interfaces with and without occluded layers. It will also prove useful to refer to Fig. 3, which plots the (continuous) solid–solid interaction energy functions $U(Y) = \int\sigma(Y)\,\mathrm{d}Y$ for interfaces with capillary condensation.

2.2. *Virgin crack interfaces*

The energy-separation function for virgin interfaces, i.e. interfaces created by separation across a plane of primary bonding in the bulk solid, in vapour environment is represented as the lower curve in Fig. 3 [10, 17]. For a condensate that wets the adsorbed surfaces, we identify the work of adhesion as that to take the system reversibly along this lower curve from the pristine (non-occluded) closed state at $Y = b_0$, $U = U_{\mathrm{i}} = {}^{\mathrm{v}}U_{\mathrm{i}}^{0}$, to the separated state at $Y = \infty$, $U = {}^{\mathrm{v}}U_{\mathrm{f}}$. The oscillations in the curves are indicative of the molecular discreteness of the intervening fluid species at the interface; the secondary minima correspond to metastable, ordered integral-layer configurations in the molecular packing [20, 37], indicated schematically at the bottom of Fig. 3.

Since the closed state of the virgin interface corresponds to the primary bonding state of the bulk solid (S), the terms in equation (9) define appropriate surface and interface energies in vacuum (0) and liquid (L)

$${}^{\mathrm{v}}W_0 = 2\gamma_{\mathrm{S}} \tag{12a}$$

$${}^{\mathrm{v}}W_{\mathrm{L}} = 2\gamma_{\mathrm{SL}} \tag{12b}$$

and likewise in equation (10) in vapour (V)

$${}^{\mathrm{v}}W_{\mathrm{V}}(p) = 2\gamma_{\mathrm{SV}}(p) = {}^{\mathrm{v}}W_{\mathrm{L}} + 2\gamma_{\mathrm{LV}}\cos\theta + {}^{\mathrm{v}}I(p). \tag{13}$$

It is of interest to examine two limiting cases of equation (13):

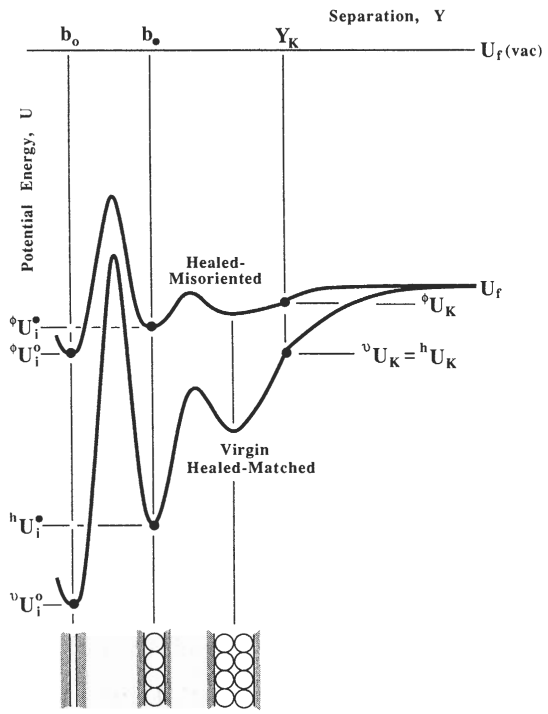

Fig. 3. Energy diagram for separation of two surfaces with capillary condensation for different interface types. Lower solid curve corresponds to virgin (v) and healed–matched (*h*) interface, upper solid curve to healed–misoriented (ϕ) interface. Oscillations (only two shown here) are indicative of discreteness in surface force functions, attributed to molecular ordering of fluid interlayers, as indicated schematically at bottom. Meniscus located at $Y = Y_K$: liquid phase at $Y < Y_K$, vapour at $Y > Y_K$. Work of separation corresponds to energy difference between initial (i) pristine state at $Y = b_\bigcirc$ (virgin, non-occluded) or $b_\bullet$ (healed, occluded) and final (f) state at $Y = \infty$. (Note final energy independent of interface type, $U_f = {}^vU_f = {}^hU_f = {}^\phi U_f$).

(i) *Zero vapour pressure*, $p/p_s = 0$. The meniscus vanishes, i.e. $r = 0$ in equation (5), as does the adsorption layer, $s = 0$, so $Y_K = b_0$ in equation (4) and ${}^vU_K = {}^vU_i^0$ (Fig. 3). Also, (neglecting possible minor interactions from any non-condensable atmospheric components) ${}^v\sigma_V = {}^v\sigma_0$, so equation (8), with equation (12a), reduces simply to

$$ {}^vW_V(0) = {}^vW_0 = 2\gamma_S. \quad (14) $$

(ii) *Saturated vapour pressure*, $p/p_s = 1$. Then $r \to \infty$ in equation (5), $Y_K \to \infty$ in equation (4), ${}^vU_K = U_f$ (Fig. 3). Thus $I(p_s) = 0$ in equation (11), so equation (13), with equation (12b), reduces to

$$ {}^vW_V(p_s) = 2(\gamma_{SL} + \gamma_{LV}\cos\theta) = 2\gamma_{SV}(p_s) \quad (15) $$

which identifies with Young's equation [6, 36]. In the event that the solid–liquid–solid adhesion is zero, i.e. ${}^vW_L = 2\gamma_{SL} = 0$, equation (15) reduces even further to ${}^vW_V = 2\gamma_{LV}\cos\theta$, in which case the adhesion is due solely to capillary forces. Note that there is nothing to exclude the condition $2\gamma_{SL} < 0$, if repulsive (e.g. hydration) forces were active.

We emphasise that the direct correspondence between work of adhesion and thermodynamic surface or interface energies in equations (12)–(15) is exclusive to virgin cracks, since it is the pristine interface that fundamentally defines the "ground state" of the bulk solid for all such energies. At the same time, the final energy state for virgin interfaces in Fig. 3 is common with that for healed interfaces, since the free surfaces experience no interaction at infinite separation: that is, $U_f = {}^vU_f = {}^hU_f = {}^\phi U_f$. Accordingly, the prefix-superscript on U_f is superfluous, and we omit it hereinafter. On the other hand, the initial energy state U_i in Fig. 3 depends very much on interface type as well as the nature and concentration of the vapour in the environment; the distinguishing superscript notation is retained in this case.

2.3. *Healed-matched crack interfaces*

Now consider healed–matched interfaces, i.e. interfaces opened and closed in the presence of vapour. We assume that the matching of opposite surfaces on closure is effected in near-atomic registry; then lattice coherence is preserved and the system retraces the virgin curve in Fig. 3, i.e. ${}^hU(Y) = {}^vU(Y)$. However, we also assume that a layer (or integral number of layers) of adsorbed molecules within the condensed phase becomes trapped at the interface (Fig. 1), so the healed configuration corresponds to a *metastable*, occluded state at $Y = b_\bullet$, $U_i = {}^hU_i^\bullet$ ($> {}^hU_i^\bigcirc = {}^vU_i^\bigcirc$, where, again, $\bigcirc$ refers to the *true* equilibrium state that would be restored if the occlusion layer could be squeezed out). This defines the initial state for subsequent re-opening of the interface. Then provided coherence is maintained during this re-opening, the interplanar force function for the healed–matched interface remains that of the virgin interface, i.e. ${}^v\sigma_L = {}^h\sigma_L$ within $b_\bigcirc < Y < Y_K$, ${}^v\sigma_V = {}^h\sigma_V$ within $Y_K < Y < \infty$.

Now let us determine the work of adhesion for healed–matched interfaces. First we expand equation (9b) to obtain

$$ \begin{aligned} {}^hW_L &= \int_{b_\bullet}^{\infty} {}^h\sigma_L \, dY = \int_{b_\bigcirc}^{\infty} {}^v\sigma_L \, dY \\ &\quad - \left\{ \int_{b_\bigcirc}^{\infty} ({}^v\sigma_L - {}^h\sigma_L)\, dY + \int_{b_\bigcirc}^{b_\bullet} {}^h\sigma_L \, dY \right\} \\ &= {}^vW_L - \gamma_h \end{aligned} \quad (16) $$

where γ_h defines an energy of formation for the occluded interface [10]. Making use of the identity between healed–matched and virgin surface force functions, the first integral term in the curly bracket vanishes and the "fault energy" reduces to

$$ \begin{aligned} \gamma_h &= \int_{b_\bigcirc}^{b_\bullet} {}^h\sigma_L \, dY \\ &= {}^hU_i^\bullet - {}^hU_i^\bigcirc \\ &= {}^hU_i^\bullet - {}^vU_i^\bigcirc \end{aligned} \quad (17) $$

which is independent of vapour pressure p. We see that the pressure-dependent residual integral in equation (11) is identical for healed and virgin interfaces

$$^{h}I(p) = \int_{Y_K(p)}^{\infty} [^{h}\sigma_V(p) - {}^{h}\sigma_L]\,dY$$

$$= \int_{Y_K(p)}^{\infty} [^{v}\sigma_V(p) - {}^{v}\sigma_L]\,dY = {}^{v}I(p). \quad (18)$$

Equation (10) then gives

$$^{h}W_V(p) = {}^{h}W_L + 2\gamma_{LV}\cos\theta + {}^{v}I(p). \quad (19)$$

Comparing equation (19) with (13), and recalling (16), we obtain $^{h}W_V(p) = {}^{v}W_V(p) - \gamma_h < {}^{v}W_V(p)$: i.e. the healed-matched curve $^{h}W_V - p$ may be generated by a simple downward translation of the "reference" virgin curve $^{v}W_V - p$ through an amount γ_h.

2.4. *Healed–misoriented crack interfaces*

Treatment of the healed–misoriented configuration is more complex, owing to the additional complication of interfacial incoherence of the mutually rotated lattices. This case is represented as the upper curve in Fig. 3. Recall that lattice rotation at $Y = \infty$ has no influence on the intersurface interaction, so the final energy U_f is as for the virgin /healed–matched curve. Given that the rotation reduces the adhesion at finite separations, i.e. $^{\phi}\sigma_L < {}^{v}\sigma_L$ within $b_{\bigcirc} < Y < Y_K$, $^{\phi}\sigma_V < {}^{v}\sigma_V$ within $Y_K < Y < \infty$, we conclude that the $^{\phi}U(Y)$ function for healed–misoriented interfaces must in general lie above the virgin/healed–matched function [10]. We suppose that entrapment of environmental species again results in an occluded interface at $Y = b_{\bullet}$,† thereby defining the initial, metastable state $U = {}^{\phi}U_i^{\bullet}$ ($> {}^{\phi}U_i^{\bigcirc} > {}^{h}U_i^{\bigcirc}$ in Fig. 3, with $\bigcirc$ again referring to true, non-occluded equilibrium states).

Now let us define an energy of formation for the healed–misoriented interface. Again expand equation (9b) thus

$$^{\phi}W_L = \int_{b_{\bullet}}^{\infty} {}^{\phi}\sigma_L\,dY = \int_{b_{\bigcirc}}^{\infty} {}^{v}\sigma_L\,dY$$

$$- \left\{ \int_{b_{\bigcirc}}^{\infty} ({}^{v}\sigma_L - {}^{\phi}\sigma_L)\,dY + \int_{b_{\bigcirc}}^{b_{\bullet}} {}^{\phi}\sigma_L\,dY \right\}$$

$$= {}^{v}W_L - \gamma_{\phi}. \quad (20)$$

Unlike in equation (16) for healed–matched interfaces, the first integral term in the curly bracket no longer vanishes, since $^{\phi}\sigma < {}^{v}\sigma$

$$\gamma_{\phi} = \int_{b_{\bigcirc}}^{\infty} ({}^{v}\sigma_L - {}^{\phi}\sigma_L)\,dY + \int_{b_{\bigcirc}}^{b_{\bullet}} {}^{\phi}\sigma_L\,dY$$

$$= ({}^{\phi}U_i^{\bigcirc} - {}^{v}U_i^{\bigcirc}) + ({}^{\phi}U_i^{\bullet} - {}^{\phi}U_i^{\bigcirc})$$

$$= {}^{\phi}U_i^{\bullet} - {}^{v}U_i^{\bigcirc} \quad (21)$$

with $\gamma_{\phi} > \gamma_h$. This first integral term represents a contribution to the fault energy from the intersurface incoherence. The identity between residual integrals noted in equation (11) for healed and virgin interfaces is now lost

$$^{\phi}I(p) = \int_{Y_K(p)}^{\infty} [^{\phi}\sigma_V(p) - {}^{\phi}\sigma_L]\,dY$$

$$< \int_{Y_K(p)}^{\infty} [^{v}\sigma_V(p) - {}^{v}\sigma_L]\,dY = {}^{v}I(p). \quad (22)$$

Then equation (10) for healed-misoriented interfaces is

$$^{\phi}W_V(p) = {}^{\phi}W_L + 2\gamma_{LV}\cos\theta + {}^{\phi}I(p). \quad (23)$$

Comparing equation (23) with (13), in conjunction with (20) and (22), we obtain

$$^{\phi}W_V(p) = {}^{v}W_V(p) - \{\gamma_{\phi} + [^{v}I(p) - {}^{\phi}I(p)]\} < {}^{v}W_V(p):$$

i.e. the healed–misoriented $^{h}W_V$–p curve is again depressed below, but is no longer necessarily parallel to, its counterpart virgin $^{v}W_V$–p curve, owing to the pressure-dependent differential square-bracket term. For the special case of "dirty surfaces", i.e. $^{\phi}W_L = 0$, at saturated vapour pressure, i.e. $^{\phi}I(p_s) = 0$ in equation (22), equation (23) reduces to

$$^{\phi}W_V(p_s) = 2\gamma_{LV}\cos\theta.$$

This limiting result describes the observed adhesion between two optical glass flats in air [22] and between glass strips in the simulated fracture experiment referred to in Section 1 [21].

3. EXPERIMENTAL

Now we describe some fracture experiments on mica interfaces to test the theoretical hypotheses of the previous section. The techniques used are described in an earlier study [10]. Our aim is to investigate the influence of intrusion of water vapour and of lattice coherence on the interface adhesion energy, specifically the dependence of W_V on relative humidity.

Specimens of muscovite mica were cut into slabs 25 mm × 10 mm, thickness 100 μm. The slabs were clamped onto a precision translation stage seated on a reflection microscope, so that the crack interfaces could be viewed *in situ*, thereby allowing constant monitoring of the crack length. Cleavage was initiated by inserting a 50 μm thick steel wedge along a near-centre separation plane. The cracks could then be made to propagate by driving the wedge at

†Actually, rotation may cause an increase in lattice spacing in addition to that from occlusion, from $b_{\bigcirc}$ to $b'_{\bigcirc}$ say in vacuum and from $b_{\bullet}$ to $b'_{\bullet}$ in fluid, because of lattice misfit between the solid surfaces and attendant reduced attractive forces (cf. grain boundary formation) [10].

a fixed speed relative to the specimen. The mechanical-energy-release rate was calculated from the conventional linear elastic fracture mechanics formula for double-cantilever beam specimens with essentially traction-free walls [14]

$$G(c) = 3Eh^2d^3/4c^4 \quad (24)$$

where $E = 170$ GPa is Young's modulus, $2h$ the wedge thickness, d the suitably "averaged" beam half-thickness ($2/d^3 = 1/d_1^3 + 1/d_2^3$ for asymmetrical beams), and c the crack length. On stopping the wedge, the crack continues to grow kinetically, but at an ever-decreasing rate, until ultimately the system attains stable equilibrium at $G_C = W_E$ [10]. By continually re-starting the wedge, several measurements of W_E could be obtained on each specimen.

Experiments were conducted in an environmental chamber at controlled partial pressures of water vapour, at 25 ± 1°C. The partial pressures were monitored with a hygrometer probe† located inside the chamber, to an absolute accuracy of ± 2–3% over the range RH = 1–100%. For RH < 20%, control was effected by introducing a container of anhydrous phosphorus pentoxide into the chamber, which was then sealed off to the laboratory atmosphere. By flowing nitrogen gas through the chamber, RH < 3% could be achieved. In this latter region the crack growth became erratic, presumably due to surface charging [3, 5], and it was difficult to obtain reproducible data [10]. For RH > 20%, a container of lithium chloride or calcium chloride solution was introduced into the closed chamber: the RH could then be regulated by varying the concentration. At all humidities, the chamber was left to stand several hours before testing, to allow the system to reach equilibrium. At saturation, capillary condensation became visible at the crack interface. In all such observations the capillary length remained sufficiently small ($\ll 25$ μm) compared to the crack length (> 1 mm) that the approximation of stress-free beams implicit in equation (24) might be considered well satisfied. Finally, for tests in liquid, the specimen was entirely immersed in distilled water. Between runs at different RH, the crack was allowed to sit for several hours before advancing the wedge, to allow the surfaces to equilibrate with each new environment.

In accordance with the theoretical treatment of the previous section, virgin, healed-matched, and healed–misoriented mica interfaces were studied: virgin interfaces by propagation of the crack along the pristine mica cleavage plane; healed–matched by initial propagation of the cleavage crack, followed by careful retraction *before* complete separation of the mica halves, and then repropagation through the closed interface; healed–misoriented similarly but *after* complete separation, with a relative rotation ≈10–20° before re-contact. The healed interfaces were all prepared in a laboratory atmosphere of RH = 40% before insertion into the chamber.

†Humidity/Temperature Indicator, Model 5165-A, Weathermeasure WEATHERtronics, Sacramento, Calif.

4. RESULTS AND ANALYSIS

Results of the adhesion energy determinations for the virgin, healed–matched and healed–misoriented crack interfaces are plotted in Fig. 4 as a function of relative humidity of water vapour. Data points indicate individual tests in vapour, hatched areas at right means and standard deviations of tests in water.

Let us note first the $W(p)$ behaviour at opposite extremes of relative humidity in Fig. 4:

(i) The mica-water data (hatched areas at right) may be used to evaluate

$$\gamma_{SL} = {}^{v}W_L/2 = 138 \pm 28 \text{ mJ}\cdot\text{m}^{-2}$$

in equation (12b),

$$\gamma_h = {}^{v}W_L - {}^{h}W_L = 124 \pm 85 \text{ mJ}\cdot\text{m}^{-2}$$

and

$$\gamma_\phi = {}^{v}W_L - {}^{h}W_L = 270 \pm 80 \text{ mJ}\cdot\text{m}^{-2}$$

in equation (16) and (20). These values are typical of interface and fault (e.g. stacking fault, grain boundary) energies in ionic-covalent solids [36, 39]. Note also at $p/p_s = 1$ that $W_V(p_s) = W_L + 2\gamma_{LV}\cos\theta$ in equations (13), (19) and (23), since $Y_K \rightarrow \infty$ in equations (18) and (22) at saturation. The arrows at right in Fig. 4 indicating $W_V(p_s)$ calculated from this limiting relation, using mean values of W_L from the water data and $\gamma_{LV} = 72$ mJ·m^{-2} (water)

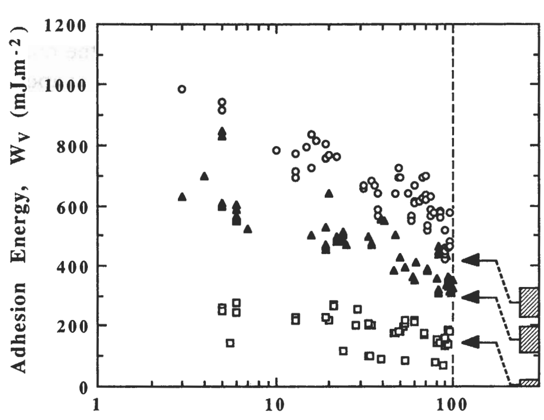

Fig. 4. Plot of measured adhesion energy W_V for mica against (logarithmic) relative humidity RH = p/p_s of water vapour. Data for crack propagation through virgin (circles), healed–matched (triangles) and healed–misoriented (squares) interfaces. Hatched areas at right axis indicate means and standard deviations of W_L for tests in liquid water. Arrows indicate corresponding values of $W_V + 2\gamma_{LV}\cos\theta$, using $\gamma_{LV} = 72$ mJ·m^{-2} and $\theta = 90°$ for mica-water. Note difference in slopes for three curves, and tendency for lowest data set to approach $2\gamma_{LV}$ asymptotically.

W_L from the water data and $\gamma_{LV} = 72\ mJ \cdot m^{-2}$ (water) [36] and $\theta \simeq 0$ (water/mica [38]), may be compared with the extrapolated W_V–p data. This identity of $W_V(p_s) - W_L$ with $2\gamma_{LV} \cos\theta$ [a generalisation of Young's equation in equation (15)] is perhaps the most direct manifestation of the existence of capillary forces in the fracture mechanics.

(ii) At the low RH end of the plot there is no indication of the plateau that would be expected if the adhesion energy W_v were to be limited by the vacuum value W_0. We have mentioned the experimental difficulties in obtaining reproducible data at low RH (<3%) necessary to establish such a limit. In terms of the energy-separation diagram of Fig. 3 this means that we are unable to quantify the energy level U_f(vac). This is not a limitation in the present study: as far as capillary condensation is concerned, it is only the relative energy levels U_f and U_i on the solid curves in that figure that have to be specified.

Now let us address the general W_V–p results in Fig. 4. We note first the monotonic decline of each data set with increasing p (at least for the virgin and healed–matched interfaces). The key to this decline lies in the residual integral terms $I(p)$ in equations (18) and (22). Since we generally expect $\sigma_V(p) > \sigma_L$, these residual integrals diminish with p: first because an increase in the vapour density (as well as in the thickness of adsorption layer, s) enhances the screening of the solid–solid interactions (as it would even if the vapour were not to form the capillary); but also because the Kelvin radius r (and s), thence Y_K in equation (4), increase with p, corresponding to a contraction in the area of crack interface outside the meniscus over which the solid–vapour–solid forces $\sigma_V(p)$ remain operative. Actually, the decrease in $W_V(p)$ should persist only while the vapour pressure is sufficiently small that Y_K remains within the range of intersurface forces. At some critical vapour pressure, $I(p) = 0$ in equations (13), (19) and (23), at which point W_V should level out at a minimum $W_L + 2\gamma_{LV} \cos\theta$. There is no clear indication as to the existence of any such critical pressure within, say RH < 90%, in any of the three data sets in Fig. 4, certainly not in the data for the virgin interfaces. The implication is that the intrinsic cleavage-plane surface forces contain a substantial long-range component: using Fig. 2 to evaluate r and conservatively assuming $s = 0$, equation (4) for Y_K yields a lower bound estimate > 10 nm for this range. Such long-range forces are consistent with Coulombic bonding between ordered interlayer potassium and uncompensated intralayer aluminium ions in the silicate sublattice, as assumed in customary descriptions of the mica crystallographic structure [2, 3, 5, 6, 40, 41].

Next consider the relative positions of the adhesion curves for virgin and healed interfaces. Recall that for healed–matched interfaces ${}^vW_V - {}^hW_V = \gamma_h$ (Section 2.3), with γ_h in equation (17) attributed exclusively to the formation energy of an occlusion layer of water molecules; and that for healed–misoriented interfaces ${}^vW_V - {}^\phi W_V = \gamma_\phi + ({}^vI - {}^\phi I)$ (Section 2.4), where γ_ϕ in equation (21) contains an *additional* contribution from loss of coherence. The latter contribution is evidently important in our results: for otherwise we would expect $\gamma_\phi = \gamma_h$ [${}^\phi\sigma_L = {}^h\sigma_L = {}^v\sigma_L$ in equations (21) and (17)], ${}^\phi I(p) = {}^hI(p) = {}^vI(p)$ [${}^\phi\sigma_L = {}^h\sigma_L = {}^v\sigma_L$ within $Y < Y_K$ and ${}^\phi\sigma_V = {}^h\sigma_V = {}^v\sigma_V$ within $Y_K < Y$ in equation (22)], in which case the data set for healed–misoriented interfaces in Fig. 4 would necessarily be coincident with that for healed–matched interfaces. We are led to conclude that the Coulombic bonding is suppressed in the ϕ configuration, due to disordering of the interlayer ionic coordination [6] [${}^\phi\sigma_V \ll {}^v\sigma_V$, ${}^\phi\sigma_L \ll {}^v\sigma_L$ at all Y and all p in equation (22)]. Note that ${}^\phi W_L$ is indeed close to zero, $\approx 5\ mJ \cdot m^{-2}$ [28], and that ${}^\phi W_V(p)$ never greatly exceeds $2\gamma_{LV} \cos\theta$ over the data range. The fact that the residual integral ${}^\phi I(p)$ in equation (23) does not reduce completely to zero is consistent with the persistence of a structure-insensitive and shorter range van der Waals component in the force-separation function [6, 16].

Indeed, it is arguable that even the less marked decrease of ${}^hW_V$ for healed-matched interfaces relative to ${}^vW_V$ may be attributable at least in part to inadvertent lattice misorientations during crack closure, notwithstanding the geometrical constraints exercised by the "built in" crack front in the partially cleaved specimen. Mutual lattice rotations of $<0.1°$ are in fact common occurrence in even the most favourable healing configurations [42]; and the evidence is that the strength of the adhesive forces is extremely sensitive to any such angular mismatch [32]. In terms of the representation of Fig. 3, such an inadvertent mismatch would be equivalent to shifting the ${}^hU(Y)$ curve to a position intermediate between ${}^vU(Y)$ and ${}^\phi U(Y)$.

5. DISCUSSION

Our theoretical analysis for surface–surface separation in a wetting condensate provides the basis for an explanation of the data in Fig. 4. Capillary condensation is thereby proposed as a critical ingredient of the fundamental adhesion characteristics of brittle solids.

Accordingly, it is instructive to consider the analysis in the context of previous models for chemically-enhanced fracture of intrinsically brittle materials. One of the earliest proposals, by Orowan [24], was that the reduced adhesion is due exclusively to adsorption of water onto the freshly cleaved walls. (Glass scientists independently developed their own version of adsorption exclusively in terms of a stress-activated hydrolytic reaction at a terminal line of bonds along the crack front [11–14].) Gaines and Tabor [25] put forward an alternative model, specifically for mica in water, arguing that the liquid acts

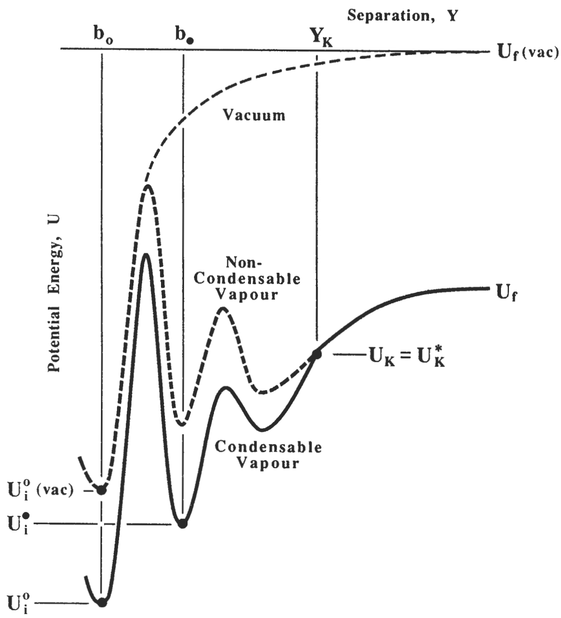

Fig. 5. Energy function for separation in vapour with capillary condensation (lower solid curve, reproduced as virgin curve from Fig. 3), in vacuum (upper dashed curve), and in hypothetical non-dielectric vapour without capillary (intermediate dashed curve). Difference in energy levels at separation $Y=\infty$ in vacuum and vapour defines adsorption energy, $2\Delta U_{\mathrm{Ad}}(p)=U_{\mathrm{f}}(\mathrm{vac})-U_{\mathrm{f}}$; difference in energy levels at separation $Y=b_{\circ}$ in presence of condensable and non-condensable vapours defines capillary energy, $\Delta U_{\mathrm{Cap}}(p)=U_{\mathrm{i}}^{\circ}-U_{\mathrm{i}}^{\circ}(\mathrm{vac})$ [plotted here as negative quantity, corresponding to a dominant $\Delta U_{\mathrm{Lap}}=-2\gamma_{\mathrm{LV}}\cos\theta$ term in equations (30) and (31)] (cf. Fig. 3).

as a dielectric medium by screening the solid–solid Coulombic attractions. Yet another school [2, 3, 5, 23], principally Derjaguin and co-workers, proposed that the adhesion in mica is due to the segregation of the interlayer ionic charge into domains, and that the effect of moisture is simply to neutralise these domains. The theory of environmental interactions in brittle fracture is notable for its diversity.

It is not the validity of these previous models that we would question here, but rather their restrictive nature. None of the above models is capable of explaining the data trends in Fig. 4 in the absence of capillary condensation. To demonstrate this, let us refer to the reconstructed potential diagram of Fig. 5, in which the energy function for separation in vapour with capillary (lower, solid curve, reproduced here from the virgin curve in Fig. 3) is plotted relative to the corresponding function in vacuum (upper, dashed curve). Then we may write the adhesion energy for interfaces with capillary condensation for either non-occluded ($U_{\mathrm{i}}=U_{\mathrm{i}}^{\circ}$) or occluded ($U_{\mathrm{i}}=U_{\mathrm{i}}^{\bullet}$) states as follows

$$W_{\mathrm{V}}=U_{\mathrm{f}}-U_{\mathrm{i}}$$
$$=W_0-\Delta U_{\mathrm{Sh}} \tag{25}$$

with W_0 the work to separate the (non-occluded or occluded) interfaces in vacuum†

$$W_0=[U_{\mathrm{f}}(\mathrm{vac})-U_{\mathrm{i}}^{\circ}(\mathrm{vac})]-[U_{\mathrm{i}}-U_{\mathrm{i}}^{\circ}] \tag{26}$$

and ΔU_{Sh} a "shielding" energy term

$$\Delta U_{\mathrm{Sh}}=[U_{\mathrm{f}}(\mathrm{vac})-U_{\mathrm{f}}]+[U_{\mathrm{i}}^{\circ}-U_{\mathrm{i}}^{\circ}(\mathrm{vac})]$$
$$=2\Delta U_{\mathrm{Ad}}+\Delta U_{\mathrm{Cap}} \tag{27}$$

where

$$2\Delta U_{\mathrm{Ad}}=U_{\mathrm{f}}(\mathrm{vac})-U_{\mathrm{f}}$$

and

$$\Delta U_{\mathrm{Cap}}=U_{\mathrm{i}}^{\circ}-U_{\mathrm{i}}^{\circ}(\mathrm{vac})$$

are formation energies of adsorption layers (two surfaces) and capillary.

We are primarily interested in $W_{\mathrm{V}}(p)$ in equation (25). The intrinsic adhesion energy W_0 in equation (26) is presumed to be pressure-independent, since $U_{\mathrm{f}}(\mathrm{vac})-U_{\mathrm{i}}^{\circ}(\mathrm{vac})$ (intrinsic separation) relates exclusively to *vacuum* and $U_{\mathrm{i}}-U_{\mathrm{i}}^{\circ}$ (occlusion) is governed by the *liquid* phase within the capillary zone (Fig. 1) during interfacial closure.

It is the shielding energy which dictates the pressure dependence of W_{V}. Suppose first that the intersurface force function is governed exclusively by the interaction between adsorbed walls, as proposed by Orowan, such that closure is effected *without* capillary formation (i.e. along the intermediate, dashed curve for non-condensable vapour in Fig. 5), thereby restoring the interface to the prevailing energy state before first separation in vacuum. In this limit $Y_{\mathrm{K}}=b$ in equation (8) (no meniscus), $U_{\mathrm{i}}^{\circ}=U_{\mathrm{i}}^{\circ}(\mathrm{vac})$, $\Delta U_{\mathrm{Cap}}=0$ in equation (27), so the shielding in equation (25) is determined exclusively by the adsorption energy $2\Delta U_{\mathrm{Ad}}$

$$W_{\mathrm{V}}(p)=\int_b^{\infty}\sigma_{\mathrm{V}}(p)\,\mathrm{d}Y$$
$$=W_0-2\Delta U_{\mathrm{Ad}}(p)\quad(\Delta U_{\mathrm{Cap}}=0). \tag{28}$$

The dependence of the adsorption energy on vapour pressure is defined by the Gibbs adsorption equation [36]

$$2\Delta U_{\mathrm{Ad}}(p)=U_{\mathrm{f}}(\mathrm{vac})-U_{\mathrm{f}}(p)$$
$$=2kT\int_0^p\Gamma(p)\mathrm{d}(\ln p) \tag{29}$$

with Γ the excess concentration of the vapour species at the solid-fluid interface, given by an appropriate

†The "reaction path" between $Y=b_{\circ}$ to ∞ for a virgin interface *in vacuum* may be represented as a simple trajectory along the upper curve in Fig. 5. The corresponding path between $Y=b_{\bullet}$ to ∞ for healed interfaces is less well defined, since the occlusion layer must be desorbed during separation.

isotherm $\Gamma = \Gamma(p)$. This equation, first used in the framework of fracture and adhesion by Maugis [31], applies universally to all interface types (virgin, healed-matched or healed–misoriented), since Γ is defined relative to the fully separated state. Thus, differentiating equation (25),

$$\mathrm{d}W_{\mathrm{V}}(p)/\mathrm{d}(\ln p) = -\mathrm{d}[2\Delta U_{\mathrm{Ad}}(p)]/\mathrm{d}(\ln p) = -2kT\Gamma(p),$$

we would predict the same slopes for all three sets of $W_{\mathrm{V}}(p)$ data in Fig. 4. That the curves are *not* parallel in Fig. 4 attests to the incompleteness of the absorption description: *capillary condensation cannot be ignored.*

Accordingly, examine the general case where the capillary term is non-zero. It is convenient to define a "dielectric screening factor" S ($\geqslant 1$) such that $S\sigma(Y)$ represents a hypothetical force between adsorbed solid surfaces in a reference non-dielectric medium. In vapour, we assume that the screening is negligible, i.e. $S_{\mathrm{V}} = 1$. In liquid, S_{L} is determined by appropriate dielectric constants [19, 20, 40, 43]: for Coulombic attractions, by the dielectric constant of the bulk liquid; for van der Waals attractions, by a coupled dielectric constant of the solid–liquid–solid system (Hamaker constant) [19, 20]. Then the capillary term may be determined in association with equation (8) as†

$$\Delta U_{\mathrm{Cap}}(p) = U_{\mathrm{i}}^{\circ}(p) - U_{\mathrm{i}}^{\circ}(\mathrm{vac}) = \Delta U_{\mathrm{Lap}} + \Delta U_{\mathrm{Diel}}(p) + \Delta U_{\mathrm{Cond}}(p) \quad (30)$$

where we define terms due to the Laplace pressure, dielectric screening of the solid–solid interaction by the liquid medium, and condensation (replacement of non-condensable vapour by liquid phase within the meniscus)

$$\Delta U_{\mathrm{Lap}} = -2\gamma_{\mathrm{LV}}\cos\theta \quad (31\mathrm{a})$$

$$\Delta U_{\mathrm{Diel}}(p) = \int_b^{Y_{\mathrm{K}}(p)} (S_{\mathrm{L}} - 1)\sigma_{\mathrm{L}}\,\mathrm{d}Y \quad (31\mathrm{b})$$

$$\Delta U_{\mathrm{Cond}}(p) = \int_b^{Y_{\mathrm{K}}(p)} [\sigma_{\mathrm{V}}(p) - S_{\mathrm{L}}\sigma_{\mathrm{L}}]\,\mathrm{d}Y. \quad (31\mathrm{c})$$

We stress that the first term is negative (attractive forces) and pressure-independent, the second and third generally positive (repulsive forces) and pressure-dependent. Differentiation of equation (25) yields

$$\mathrm{d}W_{\mathrm{V}}(p)/\mathrm{d}(\ln p) = -2kT\Gamma(p) - \mathrm{d}[\Delta U_{\mathrm{Cap}}(p)]/\mathrm{d}(\ln p);$$

such that, since the surface forces σ_{V} and σ_{L} in equations (31b) and (31c) diminish with loss of interface coherence, we expect $\mathrm{d}^{\mathrm{v}}W_{\mathrm{V}}/\mathrm{d}p < \mathrm{d}^{\phi}W_{\mathrm{V}}/\mathrm{d}p < 0$, consistent with the data trends for virgin and healed–misoriented interfaces in Fig. 4.

It is interesting to look at the special case of a non-adsorptive vapour [$s = 0$, $Y_{\mathrm{K}} = 2r\cos\theta$ in equation (4)]. Then $\Delta U_{\mathrm{Ad}} = 0$, $\Delta U_{\mathrm{Cond}} = 0$ ($\sigma_{\mathrm{V}} = \sigma_0 = S_{\mathrm{L}}\sigma_{\mathrm{L}}$) in equation (31), whence the shielding energy in equation (27) reduces to

$$\Delta U_{\mathrm{Sh}}(p) = \Delta U_{\mathrm{Lap}} + \Delta U_{\mathrm{Diel}}(p).$$

In the limit in which this vapour is replaced by its liquid phase we have $\Delta U_{\mathrm{Lap}} = 0$ (no meniscus), so the shielding energy reduces still further, to $\Delta U_{\mathrm{Sh}} = \Delta U_{\mathrm{Diel}}$ [$Y_{\mathrm{K}} = \infty$ in equation (31b)]. This latter is the case addressed by Gaines and Tabor. If dielectric screening were indeed to be the controlling factor in the reduction of adhesion energy in liquid, then equation (31b) indicates that it should also remain an important factor in vapour, *provided capillary condensation occurs* [i.e. $\theta < 90°$ in equation (4)].

It is implicit in the account of brittle fracture presented here that the crack always remains atomically sharp [17, 18, 44]: the interactions within the capillary zone do not fundamentally alter the bond structure of the intrinsic crack "tip". Elastic-sphere models of the mica structure at the cleavage plane indicate that interactive environmental molecules, including water, experience strong atomic barriers to interfacial penetration [17]. It is these barriers that are reflected in the oscillations in the energy diagram in Figs 3 and 5. The solid–fluid–solid interaction is therefore confined to a region behind the intrinsic cohesive zone. In this sense it is appropriate to interpret ΔU_{Sh} in equation (25) in terms of a pseudo-mechanical force which "shields" the crack tip from the external loading [18].‡ From the more conventional standpoint of surface chemistry, ΔU_{Sh} may be interpreted specifically as the integral of Derjaguin's disjoining pressure Π [16, 19]

$$\Delta U_{\mathrm{Sh}} = \int_b^{\infty} \Pi(Y)\,\mathrm{d}Y. \quad (32)$$

In principle, the above theoretical description should apply as well to contact as to fracture configurations. Recall our allusions in Section 1 to contact mechanics as an alternative route to the measurement of adhesion energies. There we indicated the practical restriction of that approach to healed–misoriented interfaces. It is true that contact mechanics can, with extreme care in surface–surface alignment, be used to provide some information on

†Corresponding to the difference in energy levels for a "reaction path" in Fig. 5 along the intermediate curve from $Y = b_{\circ}$ to $Y = Y_{\mathrm{K}}$ and back along the lower curve to $Y = b_{\circ}$.

‡Note that the Griffith equilibrium condition $G = W_{\mathrm{E}} = W_{\mathrm{V}}$ defined earlier may, in conjunction with equation (25), be rearranged to read $G + \Delta U_{\mathrm{Sh}} = W_0$: so that an observer at the crack tip interprets ΔU_{Sh} as a component of G, acting to balance the intrinsic cohesion W_0 ahead of the tip.

healed–matched interfaces [32]; but it is certainly unable to provide *any* information on the virgin solid–solid bonding state. As we have seen, the cleavage experiment is not subject to any such restrictions. Another disadvantage of the context experiment is that the coefficient in the relation between pulloff force and adhesion energy is not unique, depending on the relative sizes of adhesion and contact zones [33, 34] (typically, contact diameters in mica–mica adhesion are $\approx 100\,\mu$m—cf. typical capillary zone length $\ll 25\,\mu$m). This non-uniqueness has led to a spirited debate in the literature on the relative merits of different theoretical treatments of the contact problem [28]. Hence, whereas measurements of contact adhesion for mica in air confirm values in the vicinity of the surface tension of water, ${}^{\phi}W_{V} \approx 2\gamma_{LV} = 144\ \mathrm{J \cdot M^{-2}}$ [28], much of the discussion in the contact literature has been directed to the validity of the pulloff force formulas rather than to the fundamental physics and chemistry of adhesion.

Although we have focussed on mica, it is anticipated that the present analysis will be applicable to other intrinsically brittle materials, e.g. glass and sapphire, in condensable vapours. In silicate glasses the critical mechanical–energy–release rate for the repropagation of cracks at healed interfaces is only slightly higher than twice the surface tension of water over a wide range of relative humidity [45], strongly reminiscent of the behaviour for healed–misoriented mica in Fig. 4, suggesting again a dominant capillary effect. Because of the relevance of such observations to the issue of threshold behaviour in *rate-dependent* crack propagation [17, 18], there is a need for further study of capillary effects in brittle materials.

Acknowledgements—We are grateful to W. C. Carter, R. G. Horn and D. T. Smith for discussions. Funding for this work was provided by the U.S. Office of Naval Research.

REFERENCES

1. J. W. Obreimoff, *Proc. R. Soc.* **A127,** 290 (1930).
2. B. V. Derjaguin, N. A. Krotova and V. V. Karasev, *Soviet Phys. Dokl.* **1,** 466 (1956).
3. B. V. Derjaguin and M. S. Metsik, *Soviet Phys. Solid St.* **1,** 1393 (1960).
4. A. I. Bailey, *J. appl. Phys.* **32,** 1407 (1961).
5. P. J. Bryant, L. H. Taylor and P. L. Gutshall, in *Transactions of Tenth National Vacuum Symposium*, p. 21. Macmillan, New York, 1963.
6. A. I. Bailey and S. M. Kay, *Proc. R. Soc.* **A301,** 47 (1967).
7. A. I. Bailey and A. G. Price, *J. chem. Phys.* **53,** 3421 (1970).
8. R. B. Leonesio, *J. Am. Ceram. Soc.* **55,** 437 (1972).
9. D. H. Roach, D. M. Heuckeroth and B. R. Lawn, *J. Coll. Int. Sci.* **114,** 292 (1986).
10. K-T. Wan, N. Aimard, S. Lathabai, R. G. Horn and B. R. Lawn, *J. Mater. Res.* In press.
11. S. M. Wiederhorn, *J. Am. Ceram. Soc.* **50,** 407 (1967).
12. S. M. Wiederhorn, in *Fracture Mechanics of Ceramics* (edited by R. C. Bradt, A. G. Evans, D. P. H. Hasselman and F. F. Lange), Vol. 2, p. 613. Plenum, New York (1974).
13. S. M. Wiederhorn, in *Fracture of Ceramics* (edited by J. B. Wachtman), p. 217. Natnl Bureau of Standards Special Tech. Publ. 303 (1969).
14. B. R. Lawn and T. R. Wilshaw, *Fracture of Brittle Solids*, Chaps 3 & 4. Cambridge Univ. Press (1975).
15. B. R. Lawn, *Appl. Phys. Lett.* **47,** 809 (1985).
16. D. R. Clarke, B. R. Lawn and D. H. Roach, in *Fracture Mechanics of Ceramics* (edited by R. C. Bradt, A. G. Evans, D. P. H. Hasselman and F. F. Lange), Vol. 8, p. 341. Plenum, New York (1986).
17. B. R. Lawn, D. H. Roach and R. M. Thomson, *J. Mater. Sci.* **22,** 4036 (1987).
18. B. R. Lawn and S. Lathabai, *Mater. Forum* **11,** 313 (1988).
19. B. V. Derjaguin, N. V. Churaev and V. M. Muller, *Surface Forces*. Consultants Bureau, New York (1987).
20. J. N. Israelachvili, *Intermolecular and Surface Forces*. Academic Press, New York (1985).
21. S. J. Burns and B. R. Lawn, *Int. J. Fract. Mech.* **4,** 339 (1968).
22. Lord Rayleigh, *Nature, Lond.* **139,** 781 (1937).
23. B. V. Derjaguin, N. A. Krotova and V. P. Smilga, *Adhesion of Solids*, Chaps 3 & 8. Consultants Bureau, New York (1978).
24. E. Orowan, *Nature, Lond.* **154,** 341 (1944).
25. G. L. Gaines and D. Tabor, *Nature, Lond.* **178,** 1304 (1956).
26. K. Kendall, *J. Phys. D, Appl. Phys.* **4,** 1186 (1971).
27. D. Maugis and M. Barquins, *J. Phys. D, Appl. Phys.* **11,** 1989 (1978).
28. R. G. Horn, J. N. Israelachvili and F. Pribac, *J. Coll. Int. Sci.* **115,** 480 (1987).
29. K. L. Johnson, K. Kendall and A. D. Roberts, *Proc. R. Soc. Lond.* **A324,** 301 (1971).
30. B. V. Derjaguin, V. M. Muller and Yu. P. Toporov, *J. Coll. Int. Sci.* **53,** 314 (1975).
31. D. Maugis, *J. Mater. Sci.* **20,** 3041 (1985).
32. P. M. McGuiggan and J. N. Israelachvili, *Chem. Phys. Lett.* **149,** 469 (1988).
33. H. K. Christenson, *J. Coll. Int. Sci.* **121,** 170 (1988).
34. A. Fogden and L. White, *J. Coll. Int. Sci.* In press.
35. J. R. Rice, *J. appl. Mech.* **35,** 379 (1968).
36. A. W. Adamson, *Physical Chemistry of Surfaces*. Wiley, New York (1982).
37. R. G. Horn and J. N. Israelachvili, *J. Chem. Phys.* **75,** 1400 (1981).
38. L. R. Fisher, *J. Coll. Int. Sci.* **72,** 200 (1979).
39. D. Wolf and R. Benedek, in *Grain Boundary Phenomena in Electronic Ceramics: Advances in Ceramics; Vol. 1* (edited by L. M. Levinson), p. 107. Am. Ceram. Soc., Columbus, Ohio (1981).
40. A. I. Bailey and H. Daniels, *J. Phys. Chem.* **77,** 501 (1973).
41. R. F. Giese, in *Reviews in Mineralogy, Vol. 13 MICAS* (edited by S. W. Bailey), p. 105. Mineral. Soc. of America, Bookcrafters, Chelsea, Michigan (1984).
42. B. J. Hockey and B. R. Lawn, *J. Mater. Sci.* **10,** 1275 (1975).
43. U. Breitmeyer and A. I. Bailey, *Surf. Sci.* **89,** 191 (1979).
44. G. I. Barenblatt, *Adv. appl. Mech.* **7,** 55 (1962).
45. T. A. Michalske and E. R. Fuller, *J. Am. Ceram. Soc.* **68,** 586 (1985).